Electrochemical Corrosion and Wear Behavior of Hot-Dip Galvanized Steel in Soils of Northern China

Xiaoyu Jiao [1], Junhong Jia [1], Wei Chen [1,]* and **Wenlong Yang [2],***

[1] College of Mechanical and Electrical Engineering, Shaanxi University of Science & Technology, Xi'an 710021, China; bs220511001@sust.edu.cn (X.J.); jhjia@sust.edu.cn (J.J.)
[2] Department of Spine Surgery, Honghui Hospital, Xi'an Jiaotong University, Xi'an 710054, China
* Correspondence: chenweijd@sust.edu.cn (W.C.); ywl1988ywr@163.com (W.Y.)

Abstract: The study examined the corrosion and wear characteristics of hot-dip galvanized steel in complex soil environments. The results showed that hot-dip galvanized steel exhibited improved corrosion resistance characteristics. Additionally, the sliding speed was observed to influence both the coefficient of friction (COF) and the state of the worn surface. Moreover, the corrosion resistance of hot-dip galvanized steel declined as the immersion period increased. Following the incorporation of friction behavior, the galvanized layer is prone to accelerated degradation. The wear of the galvanized layer resulted in the failure of its electrochemical protection, creating a pathway for corrosion to occur on the substrate as a result of the coupling effect of corrosion and wear. The use of hot-dip galvanized steel presents challenges when exposed to a tribocorrosion environment for a prolonged period. This study lays the groundwork for future research on the maintenance cycle of industrial structures constructed primarily with hot-dip galvanized steel.

Keywords: tribocorrosion; hot-dip galvanized; EIS; soil extract; transmission tower; synergistic effect

1. Introduction

Hot-dip galvanized steels have found extensive applications in industrial applications, such as transmission towers, bottom plates of household appliances, and highway guardrails. The service life is influenced by challenging and intricate environmental conditions, such as wind and rain [1–3]. The hot-dip galvanized steel components experience various adverse effects that are not effectively mitigated. For example, the power transmission tower, when situated in an open field for an extended period, is susceptible to environmental erosion and subsequent failure [4]. The collapse of transmission towers in service around the world is largely due to corrosion and wear of the relevant hot-dip galvanized steel components [5]. The coupling effect of corrosion and wear is the key influencing factor for the failure and deterioration of hot-dip galvanized steel in power transmission towers [6–9]. To date, extensive research has been conducted on the coupling behavior of corrosion and wear (tribocorrosion behavior) of hot-dip galvanized steel [2,10–13]. The corrosion and wear characteristics of hot-dip galvanized steel in soil are notably concealed and highly detrimental.

Recently, scholars have shown an increased interest in the basic corrosive characteristics of hot-dip galvanized steel in soil. For instance, Claudia Soriano et al. [12] studied the corrosion-promoting impact of soil organics on hot-dip galvanized steel, and pointed out that soil organics, such as citric acid, could serve as corrosion promoters for hot-dip galvanized steel. Meanwhile, Stefano Rossi et al. [14] also studied the corrosion of carbon

steel in soil. They demonstrated that soil properties, especially chlorides, sulphates, and water content, were closely related to the corrosion of metal components. In addition, Ryo Hirata et al. [15] examined the corrosion characteristics of carbon steel, typically used as the base material for galvanized steel, in artificial soils with varying levels of saturation in a 3% NaCl solution. The researchers highlighted that the saturation level of the NaCl solution significantly impacted the uniformity of corrosion on carbon steel in soil. Samanbar et al. [16] investigated the corrosion characteristics of galvanized steel in an alkaline sulfate solution. Their findings indicated that sulfate ions have a detrimental impact on the protective barrier properties of the surface layers and promote prolonged corrosion activity. In the existing literature, researchers have predominantly concentrated on the basic corrosive behaviors of hot-dip galvanized steel in soil. In fact, the deterioration of galvanized steel components exposed to outdoor conditions is frequently influenced by factors such as wear in addition to corrosion. For example, the grounding components of the transmission tower are exposed to the coupling effect of corrosion and wear caused by the vibrations and wind-induced oscillations in an outdoor setting [17–21]. Limited research has been conducted on the coupling effect of corrosion and wear on galvanized steel components, as evidenced by a scarcity of studies in the literature [22–25]. The significant impact of the corrosion-wear coupling on metal components should not be overlooked. Natsis et al. [26] studied the effect of soil conditions on the wear of tillage equipment. The findings indicated that soil moisture significantly influenced equipment wear, with wear levels escalating in correlation with the expansion of cultivated land area and duration of tillage. Kostencki et al. [27] investigated the tribocorrosive characteristics of agricultural tools in soil. The results indicate that the wear strength of the parts is directly determined by the chemical elements present in the soil. Abdelrahman et al. [28] conducted a comprehensive analysis of the failure of M20 class 8.8 galvanized steel bolts (derrick bolt) in an offshore drilling station after 5 years of use. Their findings indicated that the failure was primarily attributed to fretting wear and seawater corrosion of the galvanized steel. The corrosion and wear behavior of metal components are interrelated, mutually reinforcing each other, and consequently hastening their deterioration. A. Chaouki et al. [29] have summarized the current protective measures for hot-dip galvanized steel. The main protective methods for hot-dip galvanized steel include passivation treatment, phosphating treatment, alloying treatment, and surface modification of coatings. However, each method has its drawbacks, including high costs, numerous influencing factors, and high requirements for the process. Currently, there is a focus on the corrosion and wear characteristics of metal material in the corrosive environments, such as soil. Researchers have not reached a unified and systematic conclusion due to variations in purpose and methodology. Based on these studies, it is very necessary to research the tribocorrosive behavior of metals in soil. While hot-dip galvanized steels have been utilized in practical engineering applications [30], further research is required to investigate their corrosion wear characteristics in complex environments.

This paper aims to investigate the tribocorrosive behavior of hot-dip galvanized steel in a soil extract solution. It specifically examines the effect of sliding speed on the failure process and explores the coupling mechanism between corrosion and wear. Electrochemical impedance spectroscopy (EIS) was systematically conducted on hot-dip galvanized steel and Q235 steel at various immersion durations. Additionally, the static and dynamic potential polarization of both hot-dip galvanized steel and Q235 steel were analyzed. The tribological characteristics of hot-dip galvanized steel and Q235 steel ball-disc self-matching pairs were examined under various sliding speeds in a soil extract solution. The morphology of wear and the chemical composition of the worn surface were comparatively analyzed to further confirm the tribocorrosive mechanism for hot-dip galvanized steel and

Q235 steel in soil. The study aimed to enhance the understanding of the failure mechanism of industrial components made with hot-dip galvanized steel, thereby facilitating the development of a sound maintenance plan.

2. Experimental

2.1. Materials

The hot-dip galvanized steel blocks with a size of 15 mm × 15 mm × 5 mm, exhibit a galvanized layer thickness of 100 μm, as shown in Figure 1. The comparison samples were prepared using a substrate of Q235 steel (Shanghai Xiao Huang Nano Technology Co., Ltd., Shanghai, China). The electrochemical tribocorrosive behavior of self-matching pairs of hot-dip galvanized steel was evaluated using a ball-disc reciprocating wear tester, with a 6 mm diameter ball.
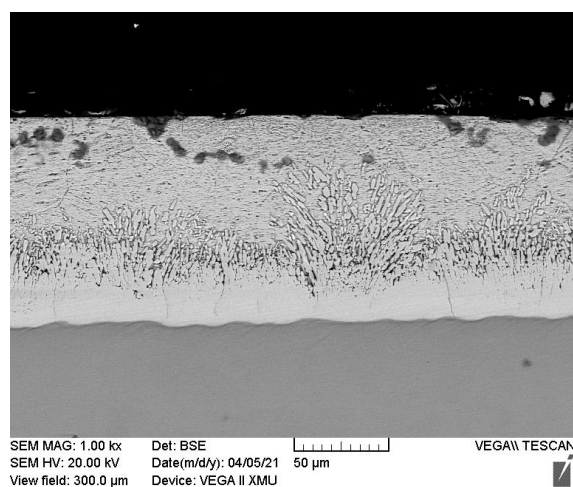
Figure 1. The thickness of hot-dip galvanized steel.

The working electrodes were prepared by embedding the sample (hot-dip galvanized steel or Q235 steel) in epoxy resin, as shown in Figure 2. Before conducting the measurements, the electrode surface was polished to achieve a mirror finish (Ra < 0.8 μm), and was subsequently cleaned using ethanol. The thin galvanized layer of hot-dip galvanized steel poses difficulties in polishing. Therefore, hot-dip galvanized steel only requires cleaning, drying, and sealing for storage.
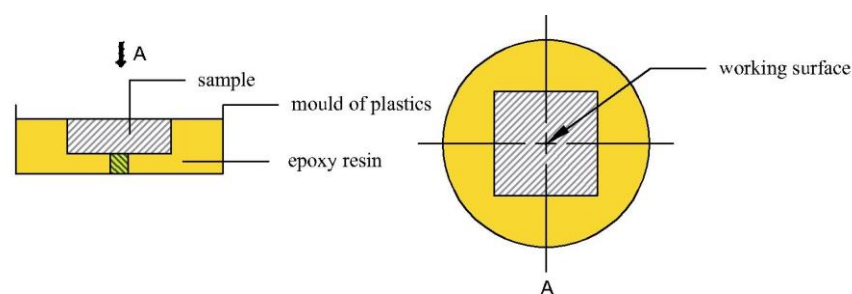
Figure 2. Schematic diagram of electrochemical test sample.

2.2. Preparation of Soil Extracts

The physical and chemical properties of various soils were investigated in our prior research [31]. In this study, a typical corrosive soil was chosen as the experimental setting (as shown in Table 1). A screen mesh with a mesh size of 2 mm was employed to screen the soil. A water–soil mixture with a ratio of soil to deionized water of 1:2.5 was then prepared and separated using a centrifuge at 4000 r/min for 1 h. Following this, the

upper clarification solution was filtered, sealed, and stored as the medium solution for the electrochemical corrosion test.

**Table 1.** Soil physical and chemical properties of typical soils.

Fe^{2+}/ mg/L	Mg^{2+}/ mg/L	Ca^{2+}/ mg/L	SO_4^{2-}/ mg/L	Cl^-/ mg/L	NO_3^-/ mg/L	Cu^{2+}/ mg/L	EC/ μs/cm	pH	Water Content/%
3.85	18.2	29.6	44.608	44.324	18.88	12	174.933	8.52	5.76

2.3. Experimental Methods

The electrochemical tribocorrosive characteristics of hot-dip galvanized steel were investigated using an electrochemical workstation (CHI604e, Chenhua, Shanghai, China) and an reciprocating friction tester (MSR-2T, Zhongkekaihua, Lanzhou, China) at room temperature. The experiments were conducted with a scan rate of 0.5 mV/s and a scanning range of −0.8 V~0.3 V for the open circuit. The polarization curve testing and electrochemical impedance spectroscopy (EIS) were conducted to monitor the corrosion over time at the open circuit potential (OCP). The cell configuration consisted of a saturated calomel electrode (SCE) and a platinum counter electrode immersed in the soil extract solution within the solution tank. The digital processing software Zview 3.1 was utilized to analyze the equivalent circuit structure and the parameters of each component.

According to the wind force scale provided by the China Meteorological Network, the study utilized the 1st soft wind, the 2nd light wind, and the 5th strong wind as the testing parameters. These were substituted with test speeds of 15 mm/s, 20 mm/s, and 25 mm/s, respectively, while applying a load of 5 N.

The test flow diagram shows the experimental procedures, as presented in Figure 3. As shown in the figure, the experiments were composed of two parts: in the first part, the electrical impedance spectroscopy test was conducted with three different immersion periods (0 days, 10 days, and 30 days). Dynamic (tribocorrosion) and static (corrosion) potential polarization curves of the samples were generated to assess the corrosion resistance of hot-dip galvanized steel. In the second part, tribocorrosion tests were performed on self-mated hot-dip galvanized steel at three different sliding speeds (15 mm/s, 20 mm/s, and 25 mm/s) at a load of 5 N to evaluate the tribocorrosive behavior of hot-dip galvanized steel in soil.
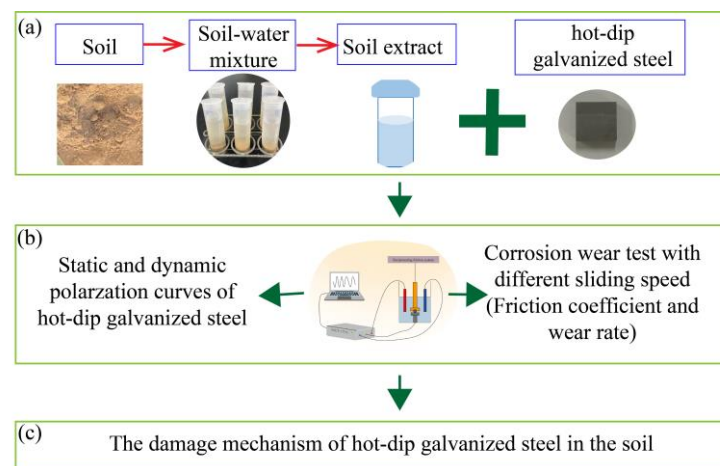
Figure 3. Flow graphs of (**a**) sample preparation, (**b**) electrochemical test and tribocorrosion test, (**c**) mechanism analysis.

2.4. Characterization

The coefficient of friction was determined using the MSR-2T reciprocating friction tester. The three-dimensional morphology and macroscopic morphology of the wear tracks were examined using a digital light microscope (DSX510, Olympus, Japan). The wear rate was calculated according to Formula (1).

$$W = V/(L \times P) \tag{1}$$

where W is the wear rate of the sample (mm^3/m·N), V is the wear volume (mm^3), L is the grinding process (m), and P is the load (N).

The scanning electron microscope (VEGA II XMU, TESCAN, Brno, Czech Republic) was employed to analyze the surface morphology and wear track. The samples were observed with X-ray diffraction (XRD, Rigaku, Tokyo, Japan) and surface-enhanced Raman spectroscopy (DXRxi, ThermFisher, Waltham, MA, USA) to examine compound composition present on the surface following the corrosion process.

3. Results

3.1. Electrochemical Corrosion Test

Figure 4 shows the electrical impedance spectra (EIS) of Q235 steel and hot-dip galvanized steel in a soil extract solution, respectively. The corresponding equivalent circuit and its related parameters are shown in Figure 5 and Table 2, respectively. The electrical impedance spectra of specimens that are not immersed in the solution are also provided in this test for comparative analysis. The results show a capacitive arc with a small radius (less than Q235) in the high-frequency range of galvanized steel during the early stages of corrosion. After immersion for 10 days, the radius of the capacitive arc expands, and the EIS curve exhibits the characteristics of Warburg impedance, displaying a "diffusion tail" in the low-frequency range. The test results suggest that immersing hot-dip galvanized steel in a solution for 10 days increases the surface corrosion layer gap, thereby creating a pathway for corrosion to occur. When the corrosion period extends to 30 days, the EIS curves of Q235 steel and hot-dip galvanized steel tend to align. Meanwhile, as shown in Table 2, the corrosion resistance of hot-dip galvanized steel exhibits a negative trend over the 30-day immersion period. This observation strongly suggests that the protective capacity of the galvanized layer on Q235 steel is inadequate within 30 days.
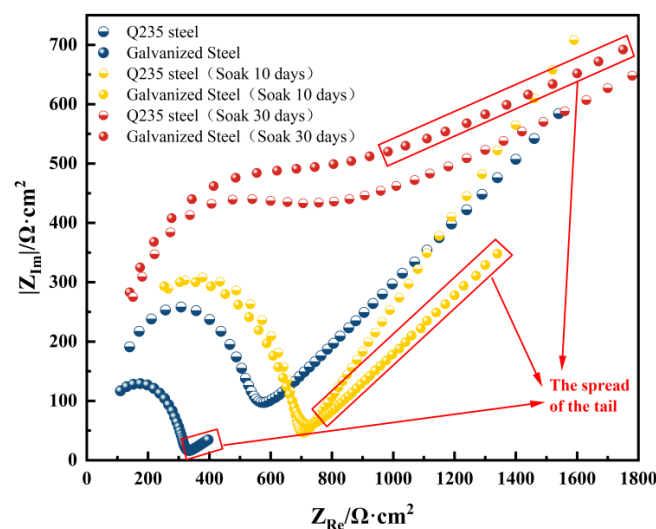

Figure 4. EIS plots of the samples with Q235 steel and hot-dip galvanized steel immersed in soil extract.
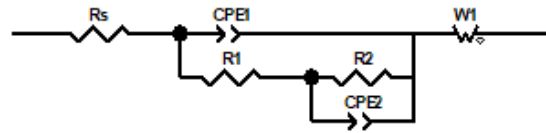
Figure 5. Equivalent circuit for Q235 steel and hot-dip galvanized steel immersed in soil extract.

Table 2. EIS data obtained by equivalent circuit simulation of Q235 steel and hot-dip galvanized steel immersed in soil extract.

| Materials	Rs [a]/$\Omega \cdot cm^2$	C_1 [b]	R_1 [c]/$\Omega \cdot cm^2$	R_2 [d]/$\Omega \cdot cm^2$	C_2 [e]	W_1
Q235	34.18	2.978×10^{-9}	395	481.8	1.047×10^{-8}	0.306
Q235 (10 d)	11.25	6.292×10^{-9}	333	320.1	5.96×10^{-8}	0.105
Q235 (30 d)	−419.2	1.387×10^{-11}	−637.3	1160	1.119×10^{-5}	0.205
Galvanized Steel	15.49	3.438×10^{-8}	244.2	34.79	5.96×10^{-8}	0.105
Galvanized Steel (10 d)	−42.37	1.209×10^{-8}	385.7	293.2	1.283×10^{-12}	0.292
Galvanized Steel (30 d)	−252.4	1.533×10^{-11}	−373.4	4399	9.896×10^{-5}	0.213

[a] Rs—Solution resistance. [b] C_1—Capacitance of rust layer. [c] R_1—Rust layer resistance. [d] R_2—Charge transfer resistance. [e] C_2—Electric double layer capacitor.

Figure 6 shows the potential dynamic polarization behavior of galvanized steel and Q235 steel in the soil extract under both dynamic and static conditions. Table 3 presents the fitting parameters determined through Tafel extrapolation. The static corrosion potentials (Ecorr) of both hot-dip galvanized steel and Q235 steel specimens (ranging from −0.123 to −0.185 VSCE) exhibit lower values compared to the dynamic corrosion potentials (ranging from −0.426 to −0.967 VSCE). Meanwhile, the static self-corrosion currents (−5.68 A/cm^2 and −5.7 A/cm^2) are also lower than the dynamic self-corrosion currents (−5.4 A/cm^2 and −5.45 A/cm^2) for both materials. The results indicate that the corrosion tendency of galvanized steel is lower than that of Q235 steel in static corrosion conditions. On the other hand, the corrosion potential and self-corrosion current of hot-dip galvanized steel and Q235 steel exhibit higher values under dynamic corrosion conditions compared to static corrosion conditions. Based on the aforementioned findings, it is evident that Q235 steel and hot-dip galvanized steel exhibit more severe damage under dynamic corrosion conditions. This suggests that wear processes enhance the corrosion propensity of metallic materials. The negative corrosion potential displacement of hot-dip galvanized steel is significantly greater than that of Q235 steel among these materials. In comparison to Q235 steel, the corrosion properties of hot-dip galvanized steel are further compromised by mechanical abrasion.

The results of the potential polarization curve and EIS show that the galvanized coating initially provides protection to Q235 steel against electrostatic corrosion. Nevertheless, as the corrosion process advances or the coupling effect of corrosion wear intensifies, the protective capability of the galvanized layer will progressively diminish or potentially cease to function.

**Table 3.** Potential dynamic polarization results of Q235 steel and hot-dip galvanized steel in soil extract.

		E_{corr}	$\log i_{corr}$	βc	βa
Static corrosion	Galvanized steel	−0.123 V	−5.68 A/cm^{-2}	27.853	23.439
	Q235	−0.185 V	−5.70 A/cm^{-2}	45.076	39.849
Dynamic wear	Galvanized steel	−0.967 V	−5.40 A/cm^{-2}	28.518	23.439
	Q235	−0.426 V	−5.45 A/cm^{-2}	41.718	38.506
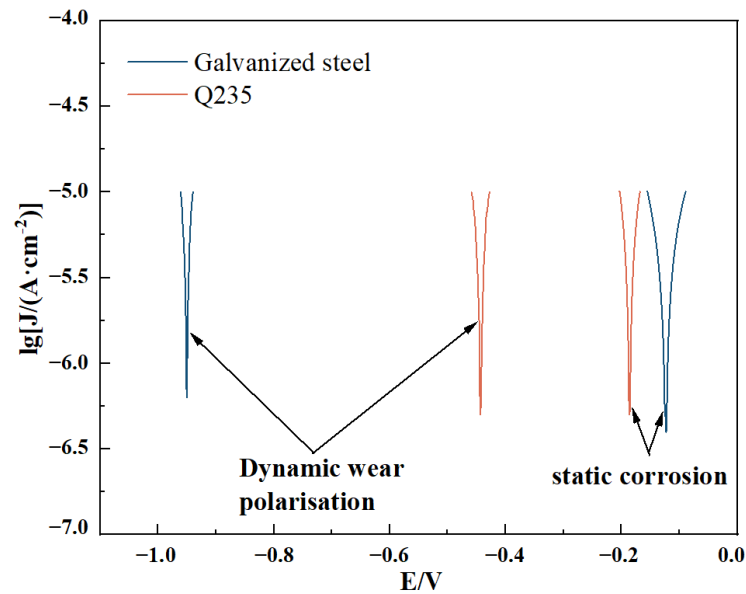
Figure 6. Potential polarization curves of Q235 steel and hot-dip galvanized steel in soil extract.

3.2. Tribological Properties

Figure 7 shows the friction coefficient curves, average friction coefficients, and wear rates of self-mated pairs consisting of hot-dipped galvanized steel and Q235 steel in the soil extract at sliding speeds of 15 mm/s, 20 mm/s, and 25 mm/s. It can be observed from Figure 7a that the friction coefficients of the hot-dip galvanized steel exceed those of Q235 steel. It can be observed from Figure 7b that the friction coefficients of hot-dip galvanized steel increase as the sliding speed increases. In contrast, the friction coefficients of Q235 steel initially increase and then slightly decrease with the increase in sliding speed. The wear rates of hot-dip galvanized steel decrease as the sliding speed increases. The findings indicate that the tribological characteristics of hot-dip galvanized steel exhibit inferior performance compared to Q235 steel in soil.
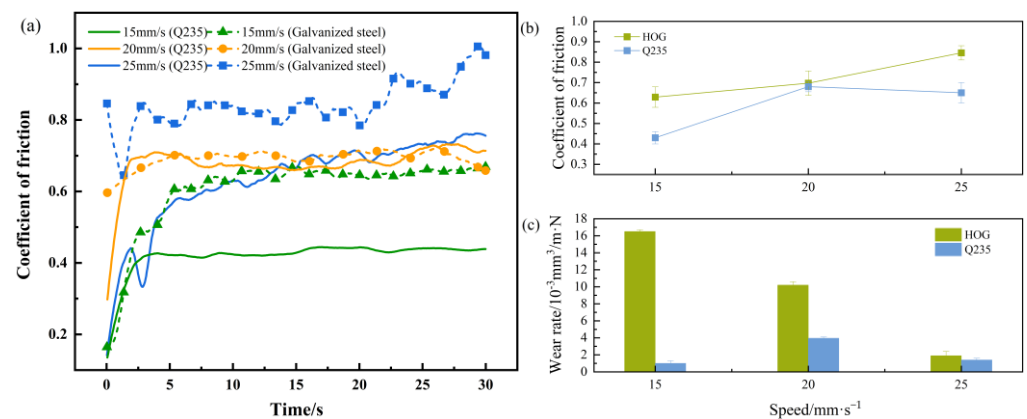
Figure 7. Variation of friction coefficient (**a**) average friction coefficient, (**b**) wear rate, (**c**) of Q235 steel and hot-dip galvanized steel at different speeds.

The morphologies of the worn surfaces resulting from the self-mated pairs of Q235 steel and hot-dip galvanized steel are illustrated in Figure 8. The figure illustrates that an increase in sliding speed results in the formation of numerous furrows on the worn surfaces of Q235 steel (Figure 8a–c), which progressively deepen. On the worn surface of Q235 steel, there is also a phenomenon characterized by the gradual reduction in thickness of wear particles. There are minimal indications of furrowing and adhesion present on the

wear surfaces of hot-dip galvanized steel (Figure 8b–f). With the escalation of sliding speed, the surface of the hot-dip galvanized steel sheet is experiencing complete spalling. The relationship between sliding speed and the oxidation rate of hot-dip galvanized steel and Q235 steel suggests a positive correlation, leading to varying degrees of surface damage [32].
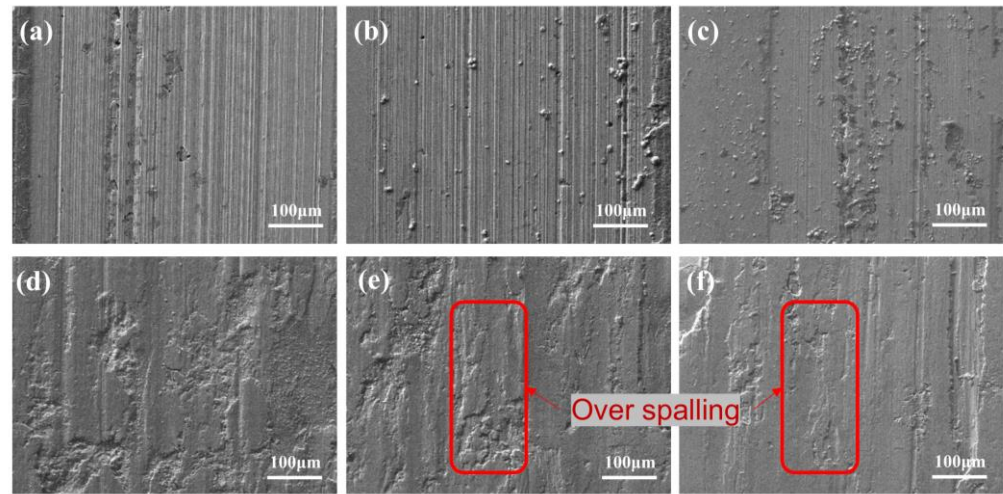
Figure 8. SEM images of wear surfaces of Q235 steel and hot-dip galvanized steel in soil extract. (**a**) Q235 steel with a sliding speed of 15 mm/s, (**b**) Q235 steel with a sliding speed of 20 mm/s, (**c**) Q235 steel with a sliding speed of 25 mm/s, (**d**) hot-dip galvanized steel with a sliding speed of 15 mm/s, (**e**) hot-dip galvanized steel with a sliding speed of 20 mm/s, (**f**) hot-dip galvanized steel with a sliding speed of 25 mm/s.

Figure 9 shows 3D topographies of worn surfaces of Q235 steel (Figure 9a–c) and hot-dip galvanized steel (Figure 9d–f). With SEM images utilized in conjunction, it becomes apparent that at a low sliding speed of 15 mm/s, the wear surface of hot-dip galvanized steel exhibits distinct grooves, smear marks, and a reduced presence of abrasive particles. As the sliding speed increases, the severity of smear marks on the wear surface of hot-dip galvanized steel gradually intensifies.
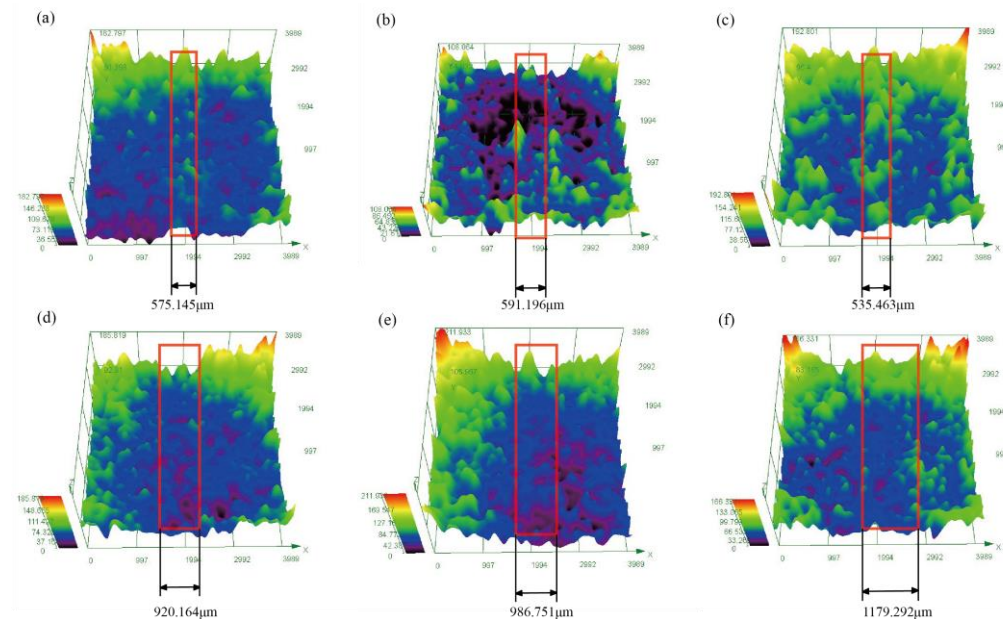
Figure 9. 3D topography of wear area and unwear areas of Q235 steel (**a**–**c**) and hot-dip galvanized steel (**d**–**f**).

The Raman spectra of the wear surfaces of hot-dip galvanized steel and Q235 steel at a sliding speed of 25 mm/s are shown in Figure 10. Since the substrate of the hot-dip galvanized steel is steel, the Raman spectrum also contains characteristic information of the substrate steel; however, due to the coverage of the zinc layer, the related peaks are relatively weak. As shown in Figure 10, at a sliding speed of 25 mm/s, the wear surface of the hot-dip galvanized steel contains $FeCl_3$, $Fe(OH)_3$, α-Fe_2O_3, and a small amount of ZnO. Comparing with the Raman spectrum of Q235 steel, it is believed that at a sliding speed of 25 mm/s, the galvanized layer of the hot-dip galvanized steel is damaged, exposing the substrate steel.
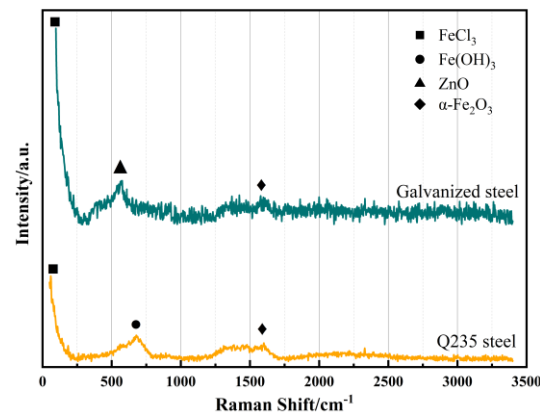
Figure 10. Raman spectra of wear track of Q235 steel and hot-dip galvanized steel at a sliding speed of 25 mm/s.

In addition, to assess the extent of damage to hot-dip galvanized steel plates at different sliding speeds, XRD tests were conducted on the wear surfaces of the materials at various sliding speeds, as shown in Figure 11. At all three speeds, the surface of the hot-dip galvanized steel exhibited Zn, ZnO, and $FeCl_2$. However, the diffraction peaks of ZnO and $FeCl_2$ at a sliding speed of 20 mm/s were the most prominent. At a sliding speed of 15 mm/s, the diffraction peak of $FeCl_2$ was almost invisible. Further evidence shows that at sliding speeds of 20 mm/s and 25 mm/s, the galvanized layer had been damaged or even removed, exposing the substrate.
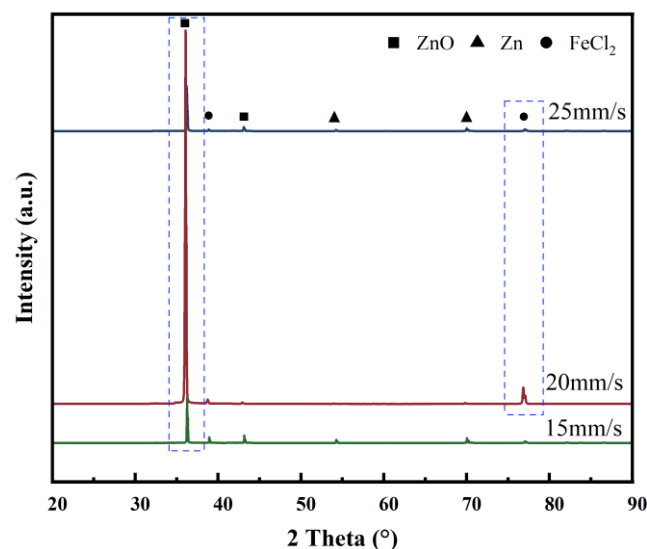

Figure 11. XRD patterns of wear tracks of hot-dip galvanized steel in soil extract at different friction rates.

4. Discussion

The corrosion mechanism of hot-dip galvanized steel in soil was previously proposed in our prior study [31]. The primary role in coating protection is attributed to $Zn(OH)_2$. However, the substrate becomes gradually exposed due to reactions like the hydrolysis of $Zn(OH)_2$. Nevertheless, hot-dip galvanized steel exhibits an increased tendency towards corrosion in soil extract over time, as suggested by electrochemical analysis results. In particular, a comparison of the EIS curves of unimmersed hot-dip galvanized steel and hot-dip galvanized steel immersed for 30 days reveals a significant presence of *Warburg* impedance characteristics. The findings indicate that the porosity of the galvanized layer surface and the stripping area of the coating-substrate cross-section were significantly higher after 30 days of corrosion. Consequently, the coating's ability to protect against corrosion was compromised [33]. Consequently, the Q235 steel substrate becomes exposed following a 30-day immersion in soil.

The potential polarization curves suggest that the dynamic corrosion tendency of hot-dip galvanized steel is more severe compared to that of pure corrosion. The wear surface of hot-dip galvanized steel at a sliding speed of 20 mm/s has been found to contain $FeCl_2$, $FeCl_3$, $Fe(OH)_3$, and α-Fe_2O_3. The low hardness of the zinc coating leads to the transfer and removal of the galvanized layer and loose abrasive particles upon repeated sliding contact. The loose abrasive particles exhibit a weak bonding force, making them prone to detachment from the surface. Higher sliding speed is associated with heightened levels of damage to the zinc layer, leading to significant zinc spalling [34]. As shown in Figure 12, loose abrasive particles and an abrasive passivation layer were observed on the wear surface. Additionally, some abrasive particles were entrained by the solution, resulting in a reduction in the wear rate.
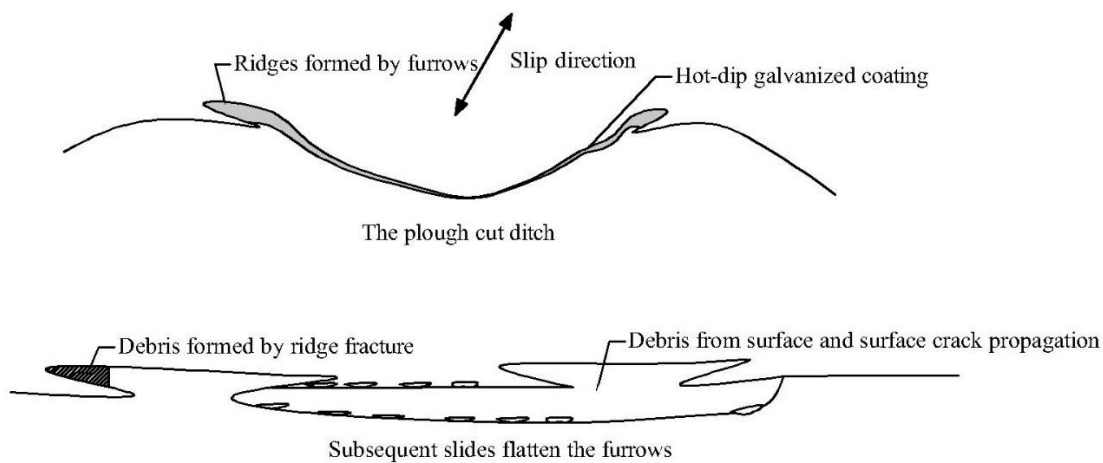
Figure 12. Schematic diagram of furrow formation and abrasive grains generated by surface crack propagation of hot-dip galvanized steel.

The increase in Cl^- concentration in the pores can be attributed to the high chlorine content in the soil and the easy adsorption of Cl^- on surface defects of the materials [35]. The adsorption capacity of chlorides on metal surfaces shows instability [36]. In particular, $ZnCl_2$ and $FeCl_3$ exhibit high solubility in water, leading to the destruction of the surface oxide film. The occurrence of stress corrosion due to the accumulation of chlorides on the surface of hot-dip galvanized steel can be attributed to working stress and thermal stress. As chloride corrosion progresses, stress concentration will form corrosion pits on the surface of the galvanized layer. The edges of these corrosion pits will generate stress concentration phenomena [37]. When external tensile stress is applied (such as stress generated during actual use due to deformation of components), the stress in the concentrated area will

be much higher than the average stress. According to fracture mechanics theory, cracks are more likely to initiate and propagate in stress concentration areas. In this case, stress corrosion cracking is more likely to occur, and cracks will continuously extend along the direction of stress concentration (such as perpendicular to the direction of tensile stress). During the wear process, the surface of hot-dip galvanized steel is subjected to repeated compression, leading to the destruction (hydrolysis) of its surface oxide film [38–42]. This breakdown exposes the substrate, creating a pathway for subsequent corrosion. Further evidence shows that at sliding speeds of 20 mm/s and 25 mm/s, the galvanized layer is damaged or even removed, exposing the substrate. Figure 13 shows the failure model of corrosion and tribocorrosion of hot-dip galvanized steel in soil. During the corrosion process, the galvanized layer initially loses electrons due to the buildup of a significant quantity of chloride ions and sulfate ions in the pores. This results in the formation of oxide layers like ZnO, which serve as a protective barrier against corrosion for the substrate. Following the introduction of friction behavior, the galvanized layer exhibits significant plastic deformation, characterized by numerous grooves, abrasive particles, and extensive spalling on the worn surface. As the sliding speed increased, the abrasive particles became progressively embedded into the surface of the hot-dip galvanized steel, leading to the squeezed and compaction of the wear debris. Moreover, the galvanized layer, serving as the anode, progressively captures electrons and generates associated compounds like ZnO and $ZnCl_2$.
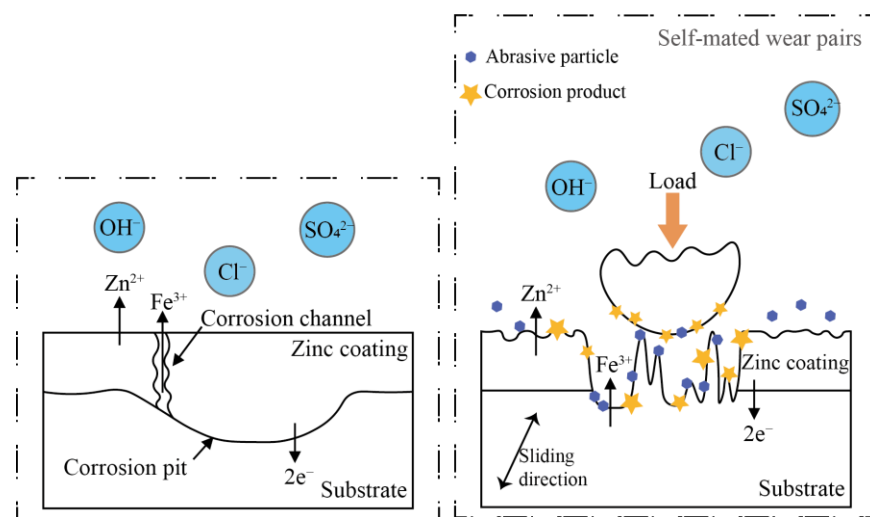
Figure 13. Corrosion and tribocorrosion of hot-dip galvanized steel in soil extract.

Throughout the friction process, the medium solution consistently removed abrasive particles and exfoliations from the surface. The exposure of the substrate to tribocorrosion led to the accumulation of a significant quantity of Cl^- and metal cations, facilitating the formation of additional chloride. This process can potentially induce stress corrosion cracking and expedite the deterioration of the galvanized layer.

The acceleration of galvanized layer failure resulting from the introduction of friction and wear behavior can be attributed primarily to the following reasons. (1) The corrosion process results in the accumulation of more chlorides, leading to an increase in the brittleness of the galvanized layer. This increased brittleness makes the galvanized layer more prone to spalling during the friction process. (2) Wear resulted in plastic deformations or dislocations on the surface, rendering the surface more reactive. (3) Prolonged tribocorrosion results in the exposure of the substrate, leading to the galvanized layer's electrochemical protection being compromised and the subsequent corrosion of the substrate.

5. Conclusions

The present study examines the tribocorrosion behavior of hot-dip galvanized steel when exposed to soil conditions. This holds significant guiding implications for further research on the maintenance cycle of outdoor equipment, such as transmission towers. The primary findings can be summarized as follows:

(1) Under identical conditions, the sliding friction and wear exacerbate the corrosion tendency of hot-dip galvanized steel more significantly than that of Q235 steel. The tribocorrosion mechanism of hot-dip galvanized steel is significantly influenced by the sliding speed. The wear performance of hot-dip galvanized steel decreases with increasing sliding speed. The primary wear mechanisms include adhesive wear, abrasive wear, and tribocorrosion;

(2) Hot-dip galvanized steel provides enhanced corrosion protection compared to Q235 steel. The addition of wear behavior results in the accelerated degradation of the galvanized layer, consequently causing the failure of cathodic protection provided by the galvanized layer;

(3) The interaction between corrosion and wear of hot-dip galvanized steel in soil accelerated the failure process. The soil contains more corrosive anions, especially Cl^-, which generates more abundant chloride causing stress corrosion, further accelerating the failure behavior. Consequently, it is essential to conduct regular maintenance on hot-dip galvanized steel when exposed to a tribocorrosive environment.

References

1. Zhang, T.; Lyu, X.; Liu, H.; Zhang, L.; Wang, J.; Gao, S. Axial performance degradation of squared CFST stubs in severe cold and acid rain area. *Constr. Build. Mater.* **2020**, *262*, 120612. [CrossRef]
2. Ferraz, G.; Rossi, B. On the fatigue behaviour of hot dip galvanized structural steel details. *Eng. Fail. Anal.* **2020**, *118*, 104834. [CrossRef]
3. Li, X.; Zhang, W.; Niu, H.; Wu, Z.Y. Probabilistic capacity assessment of single circuit transmission tower-line system subjected to strong winds. *Eng. Struct.* **2018**, *175*, 517–530. [CrossRef]
4. Yang, D.; Yan, C.; Zhang, J.; Liu, S.; Li, J. Chloride threshold value and initial corrosion time of steel bars in concrete exposed to saline soil environments. *Constr. Build. Mater.* **2021**, *267*, 120979. [CrossRef]
5. Liu, X.; Yao, H.; Wang, C.; Jin, H.; Wang, C. Failure analysis and prediction based on corrosion thinning behaviour of atmospheric tower top and volatilization line connection area. *Eng. Fail. Anal.* **2022**, *131*, 105914. [CrossRef]
6. Maher, M.; Iraola-Arregui, I.; Ben Youcef, H.; Rhouta, B.; Trabadelo, V. The synergistic effect of wear-corrosion in stainless steels: A review. *Mater. Today Proc.* **2022**, *51*, 1975–1990. [CrossRef]
7. Watson, S.; Friedersdorf, F.; Madsen, B.; Cramer, S. Methods of measuring wear-corrosion synergism. *Wear* **1995**, *181–183*, 476–484. [CrossRef]
8. Abdelrahman, M.S.; Khalifa, W.; Abdu, M.T. Failure Analysis of Fatigue Failed M20 Class 8.8 Galvanized Steel Bolt. *Eng. Fail. Anal.* **2023**, *150*, 107304. [CrossRef]

9. Bezas, M.-Z.; Jaspart, J.-P.; Vayas, I.; Demonceau, J.-F. Design recommendations for the stability of transmission steel lattice towers. *Eng. Struct.* **2022**, *252*, 113603. [CrossRef]

10. Al-Negheimish, A.; Hussain, R.R.; Alhozaimy, A.; Singh, D. Corrosion performance of hot-dip galvanized zinc-aluminum coated steel rebars in comparison to the conventional pure zinc coated rebars in concrete environment. *Constr. Build. Mater.* **2021**, *274*, 121921. [CrossRef]

11. Jin, X.; Bi, W.; Wang, L.; Qian, H. Root cause analysis of pinhole defects on painted galvanized steel panel. *Eng. Fail. Anal.* **2020**, *115*, 104598. [CrossRef]

12. Chakraborty, A.; Ghosh, R.; Sudan, M.; Mondal, A. Improvement in hot dip galvanized coating microstructure and properties by pre-metallic deposition on steel surface: A comprehensive review. *Surf. Coat. Technol.* **2022**, *449*, 128972. [CrossRef]

13. Vagge, S.; Raja, V.; Narayanan, R.G. Effect of deformation on the electrochemical behavior of hot-dip galvanized steel sheets. *Appl. Surf. Sci.* **2007**, *253*, 8415–8421. [CrossRef]

14. Rossi, S.; Pinamonti, M.; Calovi, M. Influence of soil chemical characteristics on corrosion behaviour of galvanized steel. *Case Stud. Constr. Mater.* **2022**, *17*, e01257. [CrossRef]

15. Hirata, R.; Ooi, A.; Tada, E.; Nishikata, A. Influence of the degree of saturation on carbon steel corrosion in soil. *Corros. Sci.* **2021**, *189*, 109568. [CrossRef]

16. Permeh, S.; Lau, K. Corrosion of galvanized steel in alkaline solution associated with sulfate and chloride ions. *Constr. Build. Mater.* **2023**, *392*, 131889. [CrossRef]

17. Suganya, S.; Jeyalakshmi, R. Long term study on the corrosion behaviour of buried mild steel under different native soil environments. *Mater. Today Proc.* **2021**, *47*, 957–963. [CrossRef]

18. Zeng, S.; Xu, D.; Li, D.; Li, G.; Chang, J.; Fu, C. A study on weathering steel bolts for transmission towers. *J. Constr. Steel Res.* **2020**, *174*, 106295. [CrossRef]

19. Chang, X.-D.; Peng, Y.-X.; Cheng, D.-Q.; Zhu, Z.-C.; Wang, D.-G.; Lu, H.; Tang, W.; Chen, G.-A. Influence of different corrosive environments on friction and wear characteristics of lubricated wire ropes in a multi-layer winding system. *Eng. Fail. Anal.* **2022**, *131*, 105901. [CrossRef]

20. Zhang, J.; Xie, Q. Failure analysis of transmission tower subjected to strong wind load. *J. Constr. Steel Res.* **2019**, *160*, 271–279. [CrossRef]

21. Zhao, T.; Zhang, S.; Wang, Z.; Zhang, C.; Zhang, D.; Wang, N.; Wu, C. Cavitation erosion/corrosion synergy and wear behaviors of nickel-based alloy coatings on 304 stainless steel prepared by cold metal transfer. *Wear* **2022**, *510–511*, 204510. [CrossRef]

22. Xia, D.-H.; Deng, C.-M.; Macdonald, D.; Jamali, S.; Mills, D.; Luo, J.-L.; Strebl, M.G.; Amiri, M.; Jin, W.; Song, S.; et al. Electrochemical measurements used for assessment of corrosion and protection of metallic materials in the field: A critical review. *J. Mater. Sci. Technol.* **2022**, *112*, 151–183. [CrossRef]

23. Sun, F.; Wang, X.; Han, P.; He, B. Combined EIS and BAS-BP neural network analysis of electrochemical corrosion on pipeline steel in silty soil in a Salt–Temperature coupling environment. *Int. J. Press. Vessel. Pip.* **2022**, *200*, 104807. [CrossRef]

24. Lu, C.; Ma, X.; Mills, J.E. The structural effect of bolted splices on retrofitted transmission tower angle members. *J. Constr. Steel Res.* **2014**, *95*, 263–278. [CrossRef]

25. Matlik, J.; Farris, T.; Haake, F.; Swanson, G.; Duke, G. High-frequency, high-temperature fretting-fatigue experiments. *Wear* **2006**, *261*, 1367–1382. [CrossRef]

26. Lee, C.-Y.; Lin, T.-J.; Sheu, H.-H.; Lee, H.-B. A study on corrosion and corrosion-wear behavior of Fe-based amorphous alloy coating prepared by high velocity oxygen fuel method. *J. Mater. Res. Technol.* **2021**, *15*, 4880–4895. [CrossRef]

27. Kostencki, P.; Stawicki, T.; Królicka, A. Wear of the working parts of agricultural tools in the context of the mass of chemical elements introduced into soil during its cultivation. *Int. Soil Water Conserv. Res.* **2021**, *9*, 229–240. [CrossRef]

28. Yu, Z.; Chen, M.; Li, F.; Zhu, S.; Wang, F. Synergistic effect of corrosion and wear of the 316 stainless steel in molten zinc alloy at 460 °C. *Corros. Sci.* **2020**, *165*, 108411. [CrossRef]

29. Chaouki, A.; Ben Ali, M.; El Maalam, K.; Aouadi, K.; Benabdallah, I.; El Fatimy, A.; Naamane, S. Optimizing corrosion protection: Performance comparison of Zn and Zn-Al-Mg alloys Hot-Dip galvanized coatings. *J. Alloys Compd.* **2024**, *1007*, 176371. [CrossRef]

30. Ma, H.; Zhao, B.; Liu, Z.; Du, C.; Shou, B. Local chemistry–electrochemistry and stress corrosion susceptibility of X80 steel below disbonded coating in acidic soil environment under cathodic protection. *Constr. Build. Mater.* **2020**, *243*, 118203. [CrossRef]

31. Katiyar, P.K. A comprehensive review on synergy effect between corrosion and wear of cemented tungsten carbide tool bits: A mechanistic approach. *Int. J. Refract. Met. Hard Mater.* **2020**, *92*, 105315. [CrossRef]

32. Chen, W.; Jiao, X.-Y.; Zhao, Z.-Q.; Che, Y.; Wang, S. Corrosion behavior of hot-dip zinc-coated steel in soil environment of northern China. *Electroplat. Finish.* **2021**, *41*, 1646–1652. [CrossRef]

33. Zhou, F.; Zhao, Z.; Azorin-Molina, C.; Jia, X.; Zhang, G.; Chen, D.; Liu, J.; Guijarro, J.A.; Zhang, F.; Fang, K. Teleconnections between large-scale oceanic-atmospheric patterns and interannual surface wind speed variability across China: Regional and seasonal patterns. *Sci. Total. Environ.* **2022**, *838*, 156023. [CrossRef] [PubMed]

34. Cao, C.-N. *Principles of Corrosion Electrochemistry*; Chemical Industry Press: Beijing, China, 1985.

35. Maslehuddin, M.; Al-Zahrani, M.; Ibrahim, M.; Al-Mehthel, M.; Al-Idi, S. Effect of chloride concentration in soil on reinforcement corrosion. *Constr. Build. Mater.* **2007**, *21*, 1825–1832. [CrossRef]

36. Tian, Y.; Zhang, G.; Ye, H.; Zeng, Q.; Zhang, Z.; Tian, Z.; Jin, X.; Jin, N.; Chen, Z.; Wang, J. Corrosion of steel rebar in concrete induced by chloride ions under natural environments. *Constr. Build. Mater.* **2023**, *369*, 130504. [CrossRef]

37. Savory, E.; Parke, G.; Disney, P.; Toy, N. Wind-induced transmission tower foundation loads: A field study-design code comparison. *J. Wind. Eng. Ind. Aerodyn.* **2008**, *96*, 1103–1110. [CrossRef]

38. Pu, W.; Zhang, Q.; Zhang, W.; Ren, S.; Chen, Z.; Tian, T. Flash temperature and anti-wear tribofilm growth mechanisms by asperity contact in top-ring/liner conjunction of IC engines. *Tribol. Int.* **2020**, *146*, 106186. [CrossRef]

39. Shizhuo, L.; Xiaoxia, J.; Hongyun, B.; Shu, L. Effect of environmental embrittlement on wear resistance of alloys in corrosive wear. *Wear* **1999**, *225–229*, 1025–1030. [CrossRef]

40. Xin, Y.; Song, K.; Li, Y.; Fan, E.; Lv, X. Environmentally assisted stress corrosion cracking behaviour of low alloy steel in SO^{2-} containing NaCl solution. *J. Mater. Res. Technol.* **2022**, *19*, 3255–3271. [CrossRef]

41. Xiao, Y.; Yang, L.; Zhu, W.; Zhou, Y.; Pi, Z.; Wei, Y. Delamination mechanism of thermal barrier coatings induced by thermal cycling and growth stresses. *Eng. Fail. Anal.* **2021**, *121*, 105202. [CrossRef]

42. Heldt, L.A.; Milligan, W.W.; White, C.L. *Environment-Induced Embrittlement: Stress Corrosion Cracking and Metal-Induced Embrittlement; Environmental Embrittlement of Iron Aluminide Alloys*; Michigan Technological University: Houghton, MI, USA, 1991. [CrossRef]